

**Electronic Supplementary Information (ESI) for Journal of Materials
Chemistry C.**

This journal is @ The Royal Society of Chemistry 2025

Supplementary Information

**Surface Reconstruction Approach of Nonprecious Zirconium-Enriched
Nanosheets on NiCo Nanowire Catalysts with Iron Foam Substrate for
Water Splitting†**

Mst Zakia Sultana^a, Jing Liu^a, Dongcheng Lin^a, Qin Xu^a, Maobin Pang^a, Yihan Zhen^a, Shuai
Shuai Yan^a, Baoguo Wang^{a*}

^a The State Key Laboratory of Chemical Engineering, Department of Chemical Engineering,
Tsinghua University, Beijing 100084, People's Republic of China

*Corresponding author.

E-mail address: bgwang@tsinghua.edu.cn (W. Baoguo)

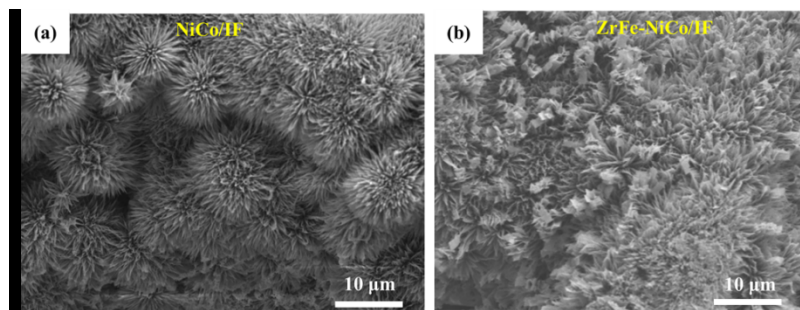


Fig. S1 SEM images of (a) NiCo/IF and (b) ZrFe-NiCo/IF.

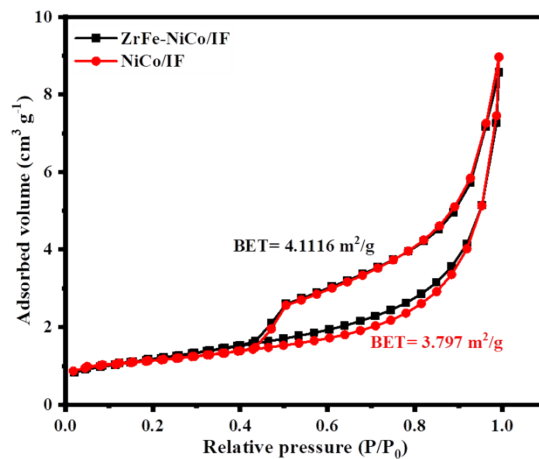


Fig. S2 Nitrogen adsorption-desorption isotherms of ZrFe-NiCo/IF and NiCo/IF.

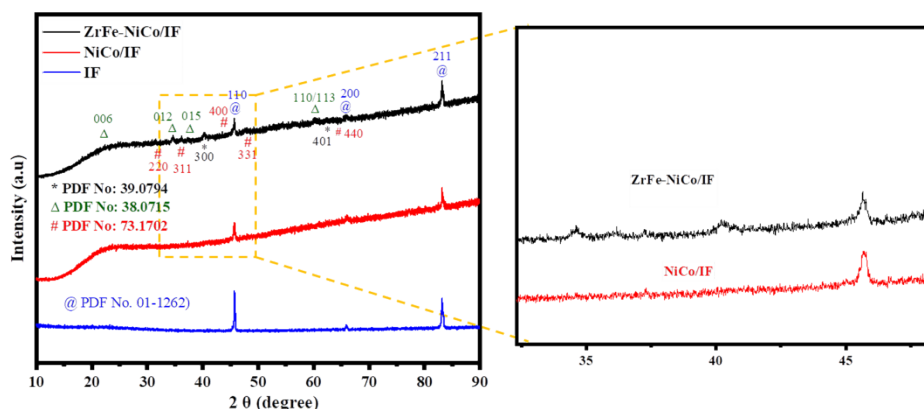


Fig. S3 XRD enlarged patterns of ZrFe-NiCo/IF and NiCo/IF.

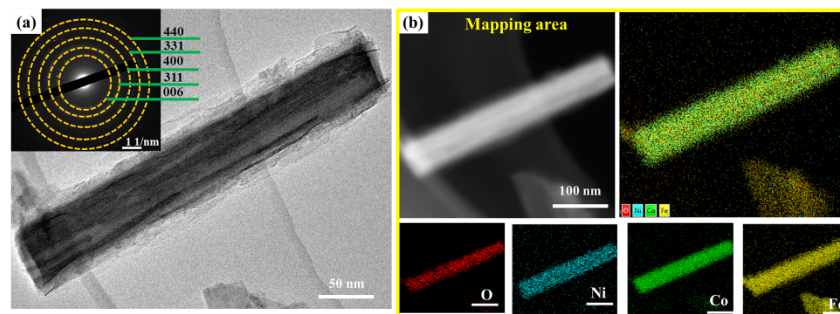


Fig. S4 (a) TEM and Inset: selected-area diffraction pattern (SAED) image of the NiCo/IF. (b) TEM-EDX mapping images of the NiCo/IF and the corresponding elemental metal distribution of O, Ni, Co and Fe.

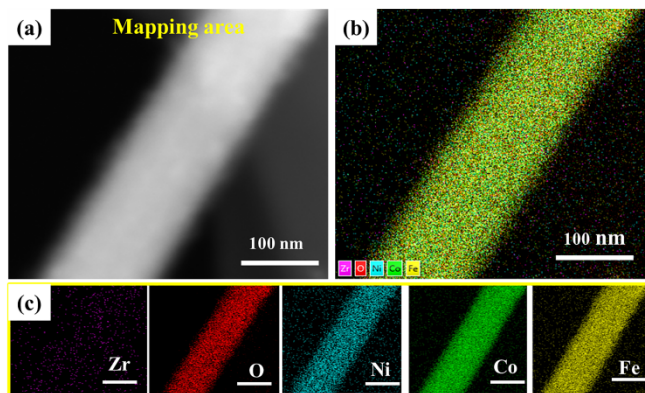


Fig. S5 (a-b) TEM-EDX mapping images of the ZrFe-NiCo/IF; (c) the corresponding element distribution of Zr, O, Ni, Co and Fe.

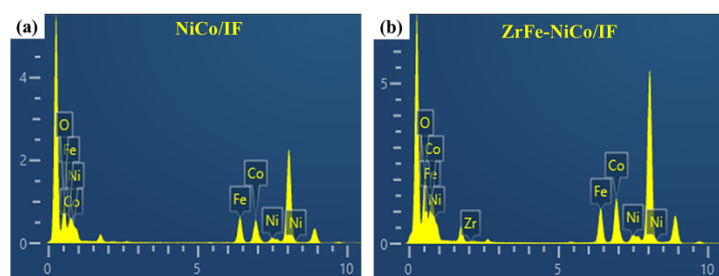


Fig. S6 EDX spectra of (a) NiCo/IF and (b) ZrFe-NiCo/IF.

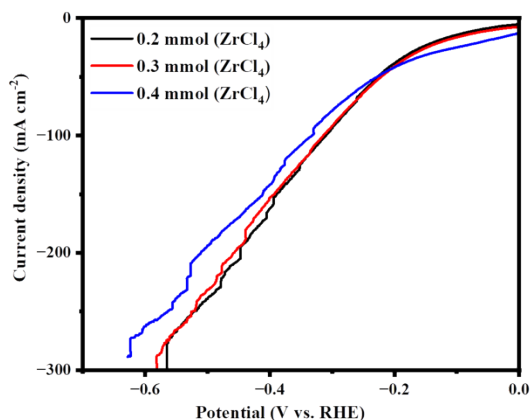


Fig. S7 HER LSV curves of ZrFe-NiCo/IF with various ratios.

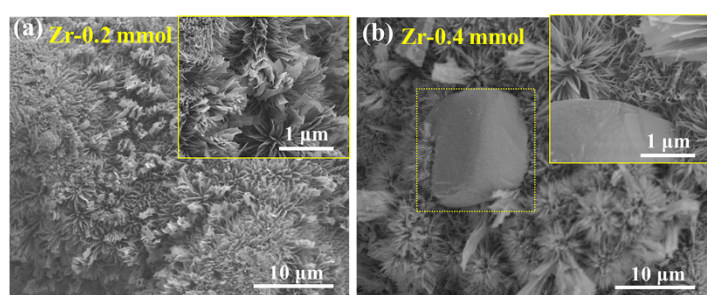


Fig. S8 SEM images of ZrFe-NiCo/IF with the various ratios of (a) Zr-0.20 mmol and (b) Zr-0.40 mmol.

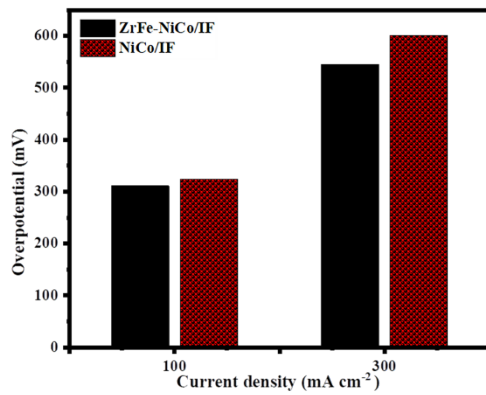


Fig. S9 The HER overpotential of ZrFe-NiCo/IF and NiCo/IF at current densities of 100 and 300 mA cm^{-2} .

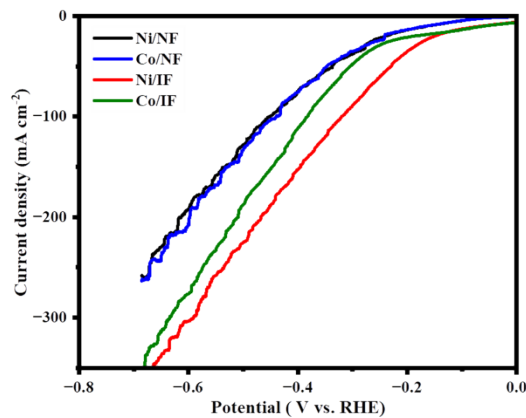


Fig. S10 HER performance, LSV curves of Ni/IF, Co/IF, Co/NF and Ni/NF.

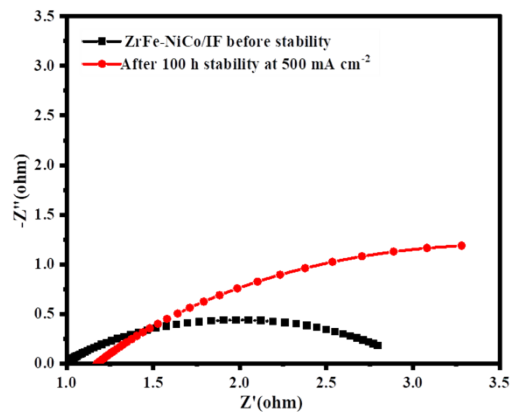


Fig. S11 Nyquist plots of ZrFe-NiCo/IF prior to and after 100 h HER durability at 500 mA cm^{-2} .

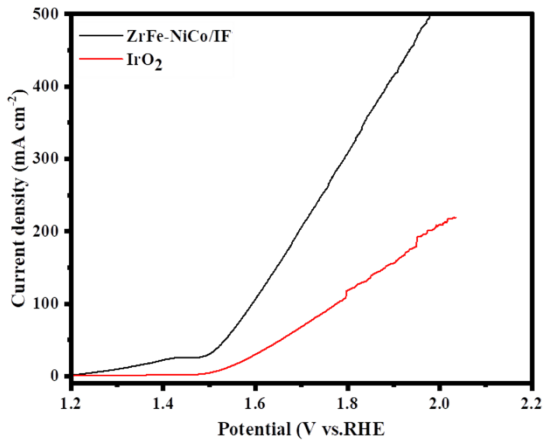


Fig. S12 OER LSV curves of ZrFe-NiCo/IF and IrO₂.

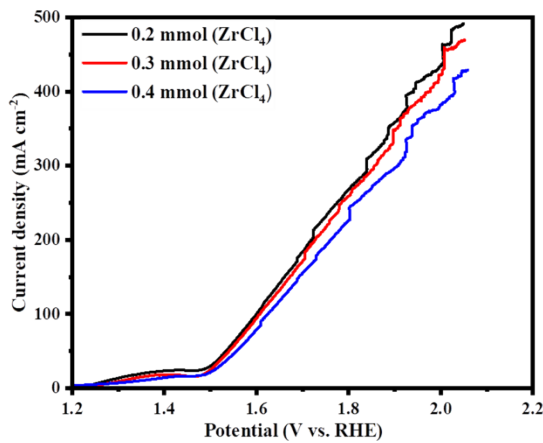


Fig. S13 OER LSV curves of ZrFe-NiCo/IF with various ratios.

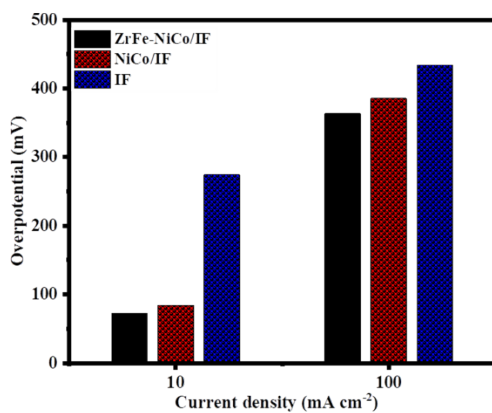


Fig. S14 The OER overpotential of ZrFe-NiCo/IF, NiCo/IF and IF at current densities of 10 and 100 mA cm^{-2} .

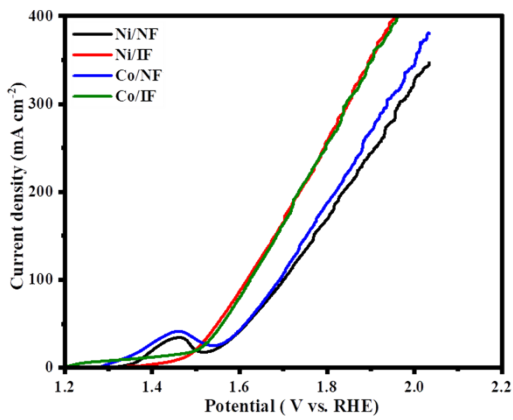


Fig. S15 OER LSV curves of Ni/IF, Co/IF, Co/NF and Ni/NF.

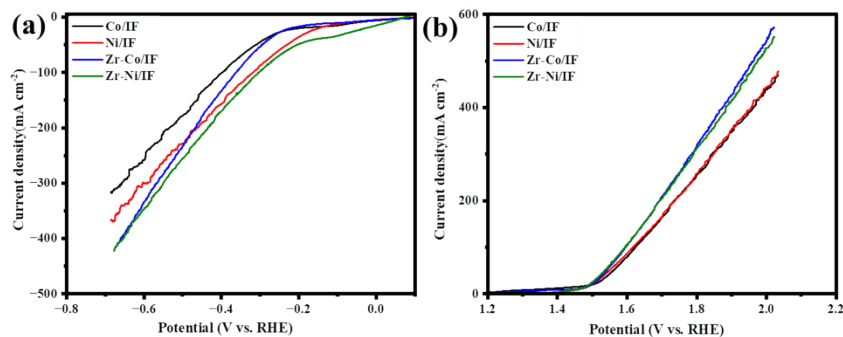


Fig. S16 (a) HER LSV curves of Co/IF, Ni/IF, Zr-Co/IF and Zr-Ni/IF and (b) OER LSV curves of Co/IF, Ni/IF, Zr-Co/IF and Zr-Ni/IF.

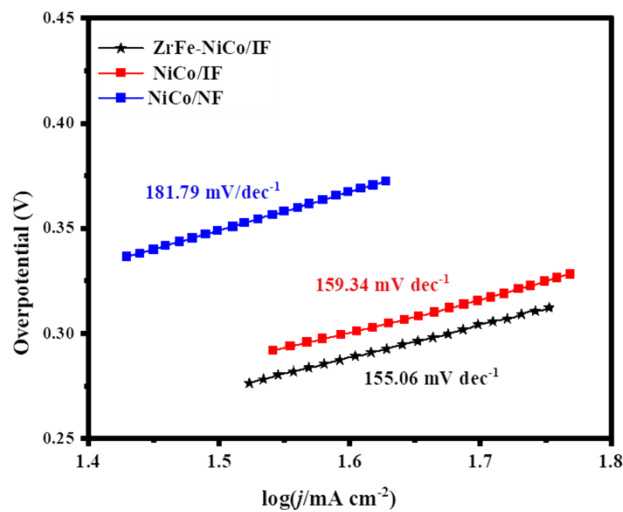


Fig. S17 Tafel slopes of ZrFe-NiCo/IF, NiCo/IF and NiCo/NF.

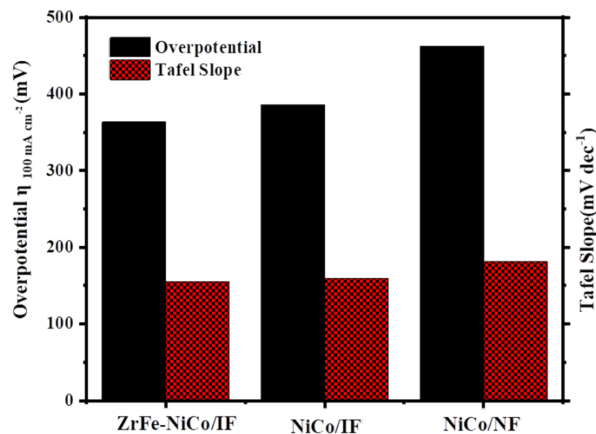


Fig. S18 Comparison of overpotentials and Tafel values with ZrFe-NiCo/IF, NiCo/IF and NiCo/NF.

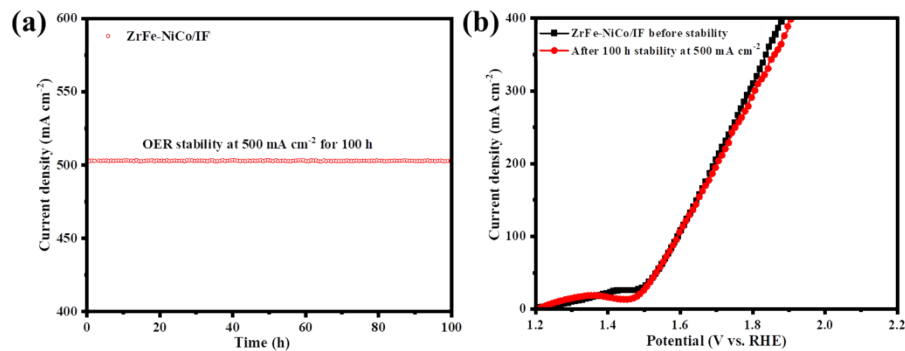


Fig. S19 OER durability tests: (a) stability tests at constant current density of 500 mA cm^{-2} for 100 h; (b) LSV curves of before and after OER 100 h stability tests at 500 mA cm^{-2} .

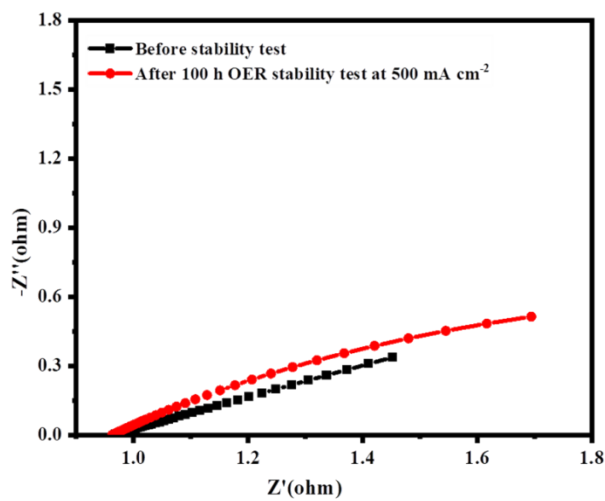


Fig. S20 Nyquist plots of the ZrFe-NiCo/IF before and after OER 100 h durability tests at 500 mA cm^{-2} .

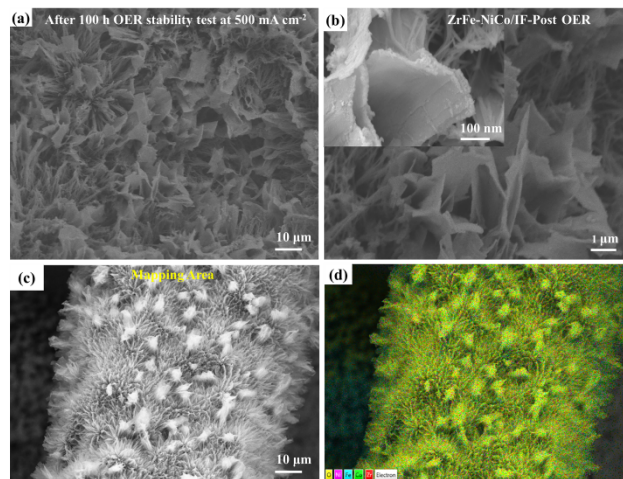


Fig. S21 OER stability at 500 mA cm^{-2} for 100 h: (a-b) SEM images and (c-d) EDX mapping area and images for ZrFe-NiCo/IF.

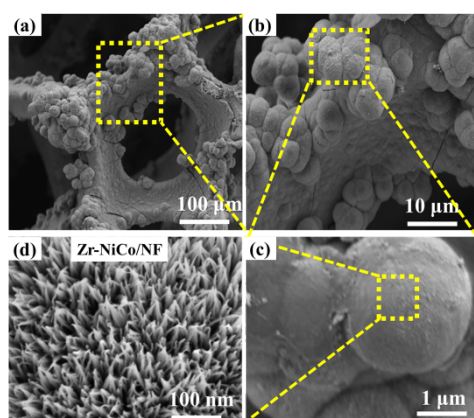


Fig. S22 SEM images of Zr-NiCo/NF (a-d).

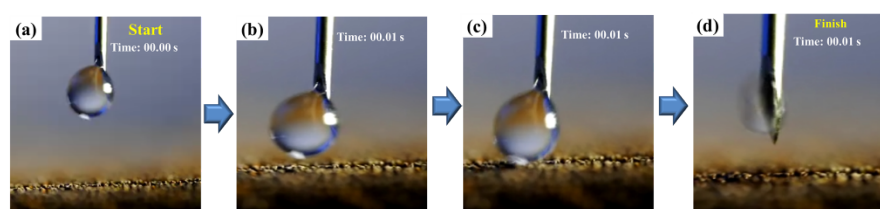


Fig. S23 (a-d) Water contact-angle measurements of ZrFe-NiCo/IF.

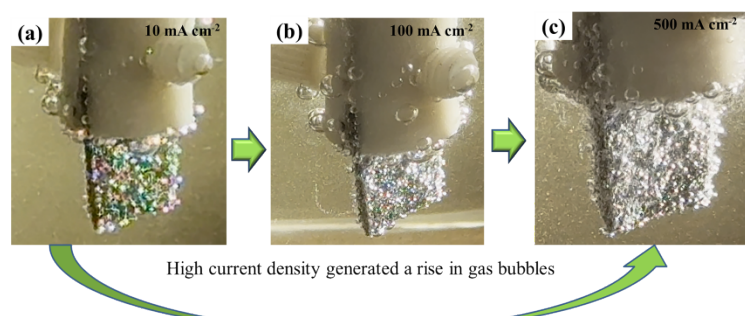


Fig. S24 (a-c) Gas bubble evolution process on the surface of ZrFe-NiCo/IF.

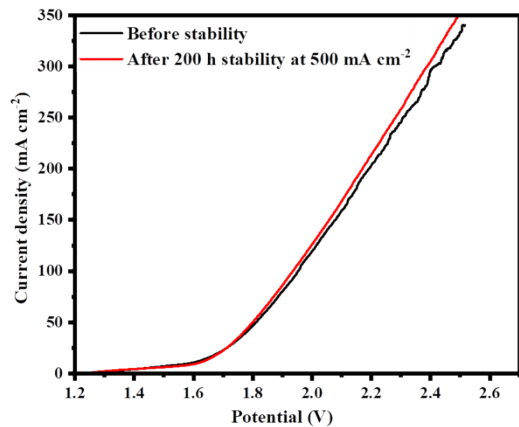


Fig. S25 ZrFe-NiCo/IF overall water splitting, LSV curve before and after 200 h stability test at 500 mA cm^{-2} .

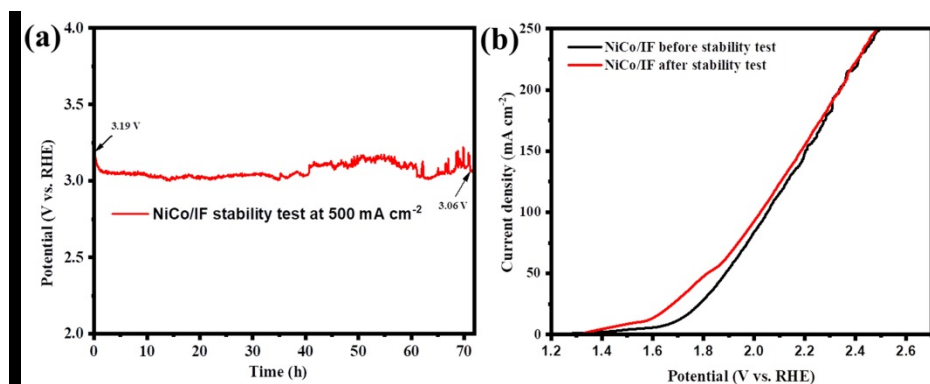


Fig. S26 (a) NiCo/IF OWS stability test at constant current density at 500 mA cm^{-2} , (b) OWS LSV curves of NiCo/IF before and after the stability test.

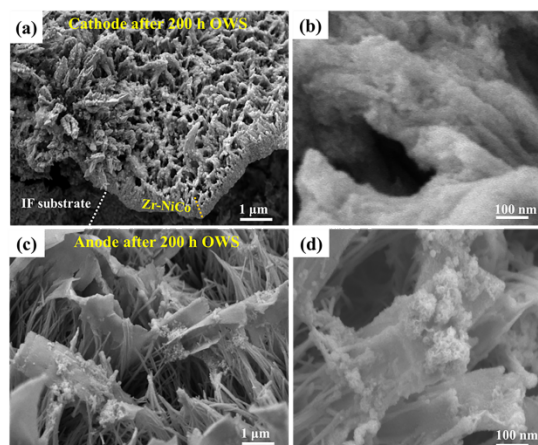


Fig. S27 SEM image of ZrFe-NiCo/IF after overall water splitting for a 200 h durability test at 500 mA cm^{-2} ; (a-b) cathode and (c-d) anode.

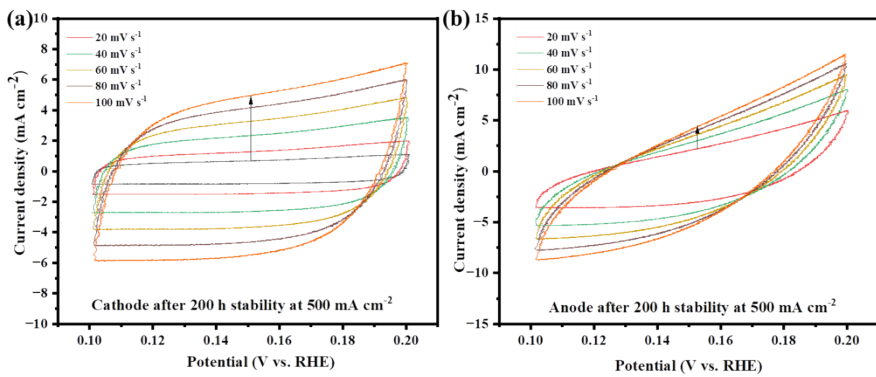


Fig. S28 Cyclic voltammograms (CV) of the samples at a scan rate of 20, 40, 60, 80 and 100 mV s⁻¹ in 1 M KOH after 200 h overall water splitting at a current density 500 mA cm⁻²; (a) cathode and (b) anode.

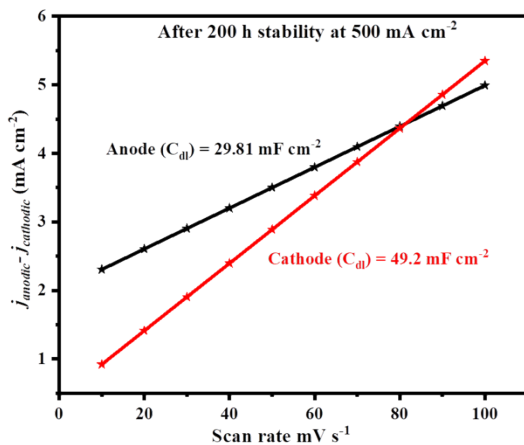


Fig. S29 The C_{dl} of anode and cathode after 200 h of water splitting at 500 mA cm⁻².

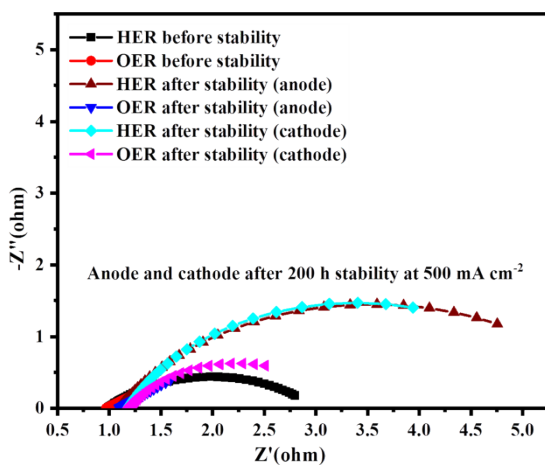


Fig. S30 Nyquist plots after the 200 h of overall water splitting at 500 mA cm⁻² as an anode and cathode.

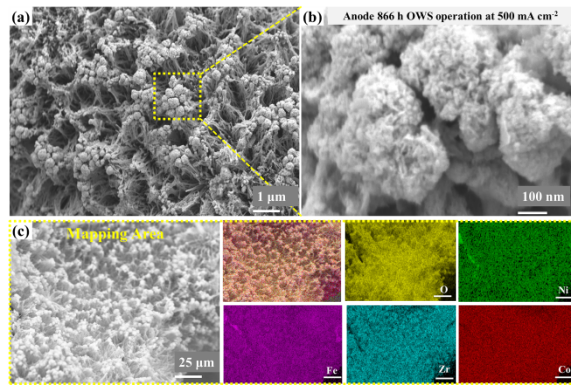


Fig. S31 As an anode ZrFe-NiCo/IF for overall water splitting after 866 h operation at 500 mA cm^{-2} , (a-b) the SEM images of ZrFe-NiCo/IF and (c) the corresponding element distribution of Zr, O, Ni, Co and Fe.

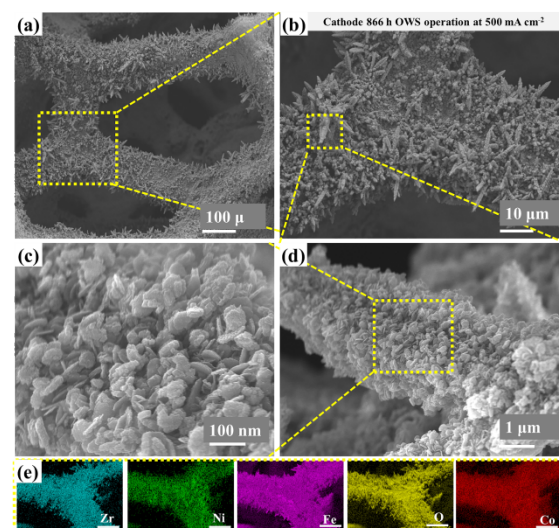


Fig. S32 As a cathode, ZrFe-NiCo/IF for overall water splitting after 866 h operation at 500 mA cm^{-2} , (a-d) the SEM images and (e) the corresponding element distribution of Zr, O, Ni, Co and Fe.

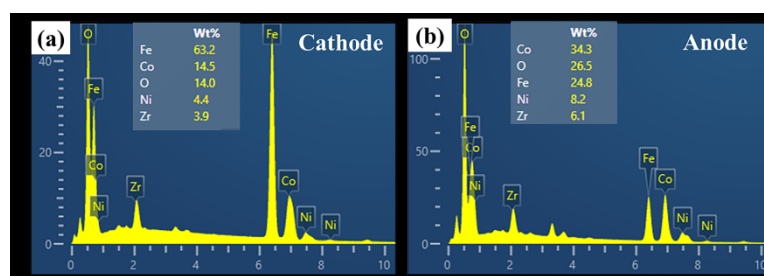


Fig. S33 EDX spectra of the ZrFe-NiCo/IF as a cathode and anode for overall water splitting after 866 h of operation at a current density of 500 mA cm^{-2} .

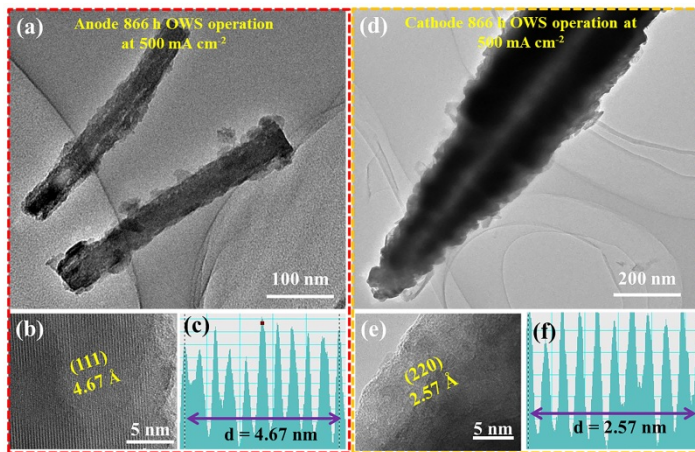


Fig. S34 ZrFe-NiCo/IF catalysts after overall water splitting for 866 h of operation at 500 mA cm^{-2} , anode: (a) TEM image, (b) HR-TEM image, (c) interplanar crystal spacing. Cathode: (d) TEM image, (e) HR-TEM image, (f) interplanar crystal spacing.

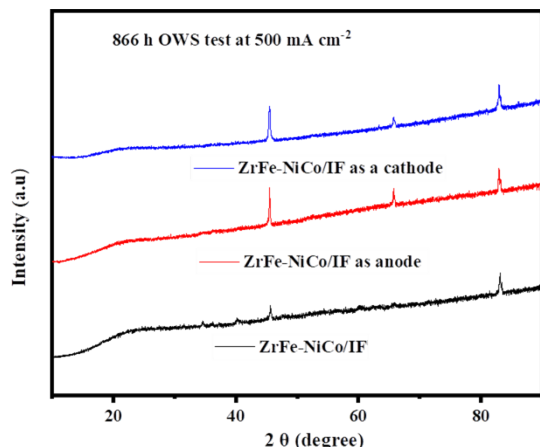


Fig. S35 XRD patterns of ZrFe-NiCo/IF before stability and after long-term stability as an anode and cathode.

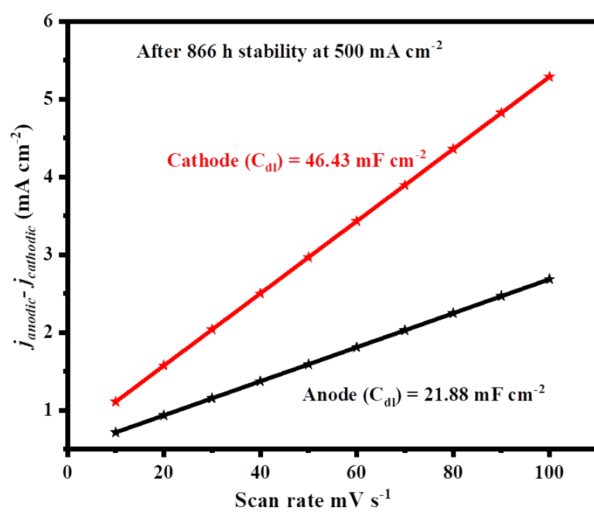


Fig. S36 The C_{dl} of anode and cathode after 866 h of water splitting at 500 mA cm^{-2} .

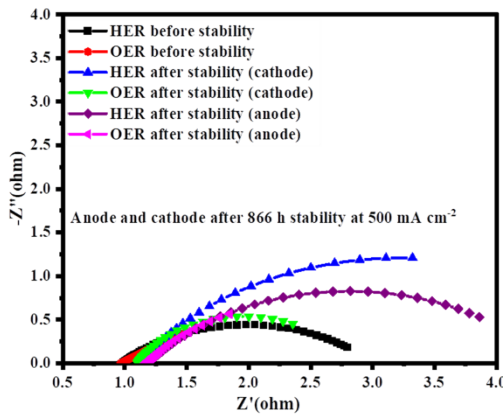


Fig. S37 Nyquist curves before and after 866 h stability test at 500 mA cm^{-2} as anode and cathode.

Table S1. The elemental binding energy from XPS.

	Ni	Co	Fe	Zr
ZrFe-NiCo/IF	854.13/859.91 & 871.51/877.00	779.3/784.00 & 795.04/800.61	709.15/712.98 & 717.4/722.77	180.32 & 182.76
NiCo/IF	854.13/860.65 & 871.88/877.77	780.01/784.76 & 795.38/801.22	709.75/713.63 & 718.19/723.46	
IF	-	-	710.57 / 714.37 & 718.95 / 724.20	

Table S2. Elemental analysis of present metals by ICP-OES.

Sample	Co (mg)	Ni (mg)	Zr (μg)
NiCo/IF	2.54	2.54	-
ZrFe-NiCo/IF	2.828	2.804	11.897

Table S3. Summary of the EIS results of before and after stability test for 200 h and 866 h at current density 500 mA cm^{-2} as an anode and cathode (HER EIS and OER EIS).

Sample (HER)	R _{ct} (Ω)	Sample (OER)	R _{ct} (Ω)
Before test HER	1.8	Before test OER	0.485
Cathode HER- 200 h stability	2.72	Cathode OER- 200 h stability	1.32
Anode HER- 200 h stability	3.61	Anode OER- 200 h stability	0.49
Cathode HER- 866 h stability	2.19	Cathode OER- 866 h stability	1.25
Anode HER- 866 h stability	2.65	Anode OER- 866 h stability	0.68

Table S4. The practical application base alkaline water electrolyzer comparison of stability test vs. current density, cell voltage and operation condition with recent reports.

Electrocatalysts	Electrolyte	Cell voltage (V)	Current density (mA cm ⁻²)	Temp. (C)	Stability (h)	Test cell setup	Ref
ZrFe-NiCo/IF	6 M KOH	1.94	500	80	233	AELWE	This work
Ir@Zr-CoP	1 M KOH	1.8	500	60	150	AEMWE	¹
NiCoFe–NDA	0.1M KOH	1.8-2	325	50	100	AEMWE	²
NiMo/CoMn/Ni	6 M KOH	1.717	100	80	50	AELWE	³
Ru-Ni ₂ P/Fe ₂ P	1 M KOH +seawater	2	500	60	100	AEMWE	⁴
Cr ₂ O ₃ –CoO _x	seawater	2.1	500	25	100	PEMWE	⁵
IrO ₂ (-) Pt/C(-)	Water	2.29	500	50	3	AEMWE	⁶
Co ₃ S ₄ /NF Cu _{0.81} Co _{2.19} O ₄ NS/NF	1 M KOH	2	500	45	64	AEMWE	⁷

References

- 1 Ngo, Q. P.; Nguyen, T. T.; Le, Q. T. T.; Lee, J. H.; Kim, N. H., Unveiling the Synergistic Effect of Atomic Iridium Modulated Zirconium-Doped Pure Phase Cobalt Phosphide for Robust Anion-Exchange Membrane Water Electrolyzer. *Advanced Energy Materials* **2023**, *13* (44).
- 2 Yue, K.; Liu, J.; Zhu, Y.; Xia, C.; Wang, P.; Zhang, J.; Kong, Y.; Wang, X.; Yan, Y.; Xia, B. Y., In situ ion-exchange preparation and topological transformation of trimetal-organic frameworks for efficient electrocatalytic water oxidation. *Energy & Environmental Science* **2021**, *14* (12), 6546-6553.
- 3 Cao, X.; Yang, Z.; Wu, X.; Wang, X.; Teng, X.; Yun, J.; Zhang, J.; Liang, X., Multilayered NiMo/CoMn/Ni Cathodic Electrodes with Enhanced Activity and Stability toward Alkaline Water Electrolysis [J]. *ACS Applied Materials & Interfaces* **2023**, *15* (28), 34181-34194.
- 4 Li, X.; Wu, T.; Li, N.; Zhang, S.; Chang, W.; Chi, J.; Liu, X.; Wang, L., Vertically Staggered Porous Ni₂P/Fe₂P Nanosheets with Trace Ru Doping as Bifunctional Electrocatalyst for Alkaline Seawater Splitting. *Advanced Functional Materials* **2024**, *34* (34), 2400734.
- 5 Guo, J.; Zheng, Y.; Hu, Z.; Zheng, C.; Mao, J.; Du, K.; Jaroniec, M.; Qiao, S.-Z.; Ling, T., Direct seawater electrolysis by adjusting the local reaction environment of a catalyst. *Nature Energy* **2023**, *8* (3), 264-272.
- 6 Xu, D.; Stevens, M. B.; Cosby, M. R.; Oener, S. Z.; Smith, A. M.; Enman, L. J.; Ayers, K. E.; Capuano, C. B.; Renner, J. N.; Danilovic, N.; Li, Y.; Wang, H.; Zhang, Q.; Boettcher, S. W., Earth-Abundant Oxygen Electrocatalysts for Alkaline Anion-Exchange-Membrane Water Electrolysis: Effects of Catalyst Conductivity and Comparison with Performance in Three-Electrode Cells. *ACS Catalysis* **2019**, *9* (1), 7-15.
- 7 Park, Y. S.; Yang, J.; Lee, J.; Jang, M. J.; Jeong, J.; Choi, W.-S.; Kim, Y.; Yin, Y.; Seo, M. H.; Chen, Z.; Choi, S. M., Superior performance of anion exchange membrane water electrolyzer: Ensemble of producing oxygen vacancies and controlling mass transfer resistance. *Applied Catalysis B: Environmental* **2020**, *278*, 119276.